Journal of Alloys and Compounds 509 (2011) 8522–8529

Contents lists available at ScienceDirect

Journal of Alloys and Compounds

journal homepage: www.elsevier.com/locate/jallcom

Development of new magnesium based alloys and their nanocomposites

Md Ershadul Alam[a], Samson Han[b], Quy Bau Nguyen[b], Abdel Magid Salem Hamouda[a], Manoj Gupta[b,*]

[a] Department of Mechanical and Industrial Engineering, College of Engineering, Qatar University, Doha, 2713, Qatar
[b] Department of Mechanical Engineering, National University of Singapore, 9 Engineering Drive 1, Singapore, 117576, Singapore

ARTICLE INFO

Article history:
Received 7 April 2011
Received in revised form 1 June 2011
Accepted 6 June 2011
Available online 15 June 2011

Keywords:
Magnesium alloy
Nanocomposite
AZ31
Al_2O_3
Nanoparticles

ABSTRACT

In the present study, 1 and 2 wt.% of aluminum were successfully incorporated into magnesium based AZ31 alloy to develop new AZ41 and AZ51 alloys using the technique of disintegrated melt deposition. AZ41–Al_2O_3 and AZ51–Al_2O_3 nanocomposites were also successfully synthesized through the simultaneous addition of aluminum (1 and 2 wt.%, respectively) and 1.5 vol.% nano-sized alumina into AZ31 magnesium following same route. Alloy and composite samples were then subsequently hot extruded at 400 °C and characterized. Microstructural characterization studies revealed equiaxed grain structure, reasonably uniform distribution of particulate and intermetallics in the matrix and minimal porosity. Physical properties characterization revealed that addition of both aluminum and nano-sized alumina reduced the coefficient of thermal expansion of monolithic AZ31. The presence of both Al and nano-sized Al_2O_3 particles also assisted in improving overall mechanical properties including microhardness, engineering and specific tensile strengths, ductility and work of fracture. The results suggest that these alloys and nanocomposites have significant potential in diverse engineering applications when compared to magnesium AZ31 alloy.

1. Introduction

The finite oil and gas reserves and global inclination to reduce CO_2 emissions have been catalytic in directing the attention of research scientists to look for light weight materials. Magnesium, with a density of 1.738 g/cm^3, is the lightest engineering metal available in the earth and is about two-thirds of the density of aluminum (2.70 g/cm^3) and one-quarter of that of iron (7.87 g/cm^3) [1]. Hence, its use is gaining significance in certain key engineering applications, particularly in electronic, automobile and aviation industries where weight is one of the most important criteria of material selection [2–5]. Besides low density, magnesium based materials exhibit good specific mechanical properties, machinability, castability, weldability, thermal stability, damping and resistance to electromagnetic radiation [6]. However, as magnesium has low ductility, modulus of elasticity and limited strength and creep resistance at elevated temperature, it cannot be extensively applied in structural applications [5–7]. Therefore, magnesium is rarely used in its pure form. Instead, it is usually alloyed with other elements like aluminum, zinc, silver and zirconium to improve its properties like corrosion resistance and ductility [1,8–10]. Among these alloying constituents, the addition of aluminum seems to have the most favorable effect on magnesium, exhibiting much greater strength and hardness [1]. Even though there has been extensive research and characterization on magnesium–aluminum alloys, it has mainly focused on specific compositions, like AZ31 (3 wt.% Al, 1 wt.% Zn, remaining Mg), AZ61 (6 wt.% Al, 1 wt.% Zn, remaining Mg) and AZ91 (9 wt.% Al, 1 wt.% Zn, remaining Mg) [1,6,9–12]. Results of open literature search show that only a few research groups have worked on developing and characterizing AZ41 sheets, mainly by twin-roll-cast technique [13–16], while Kim et al. [17] synthesized and characterized AZ51 alloys that contained pure Sn up to 9 wt.%. No results are reported in which investigators have synthesized AZ41 and AZ51 alloys by incorporating 1 and 2 wt.% elemental Al, respectively, by superheating with AZ31 using DMD technique. Hence, this study aims to develop these Mg based alloys by DMD technique and subsequently characterize to investigate their physical, microstructural, thermal and mechanical properties.

Metal matrix composites (MMCs) have gained increasing popularity as their properties could be altered accordingly by changing the matrix and its reinforcements. This is particularly useful in engineering applications especially when properties of traditional materials like metals, polymers and ceramics are not able to match with expected properties. In recent studies, it has been observed that the addition of nano-sized reinforcements such as ceramic oxides, SiC and carbon nanotubes can lead to a simultaneous increase in strength and ductility of magnesium [6,18,19]. Among all the reinforcements, it can be observed from the study that the 1.5 vol.% addition of nano-sized alumina particulates in magnesium based matrix showed the best overall combination

* Corresponding author. Tel.: +65 6516 6358; fax: +65 6779 1459.
E-mail address: mpegm@nus.edu.sg (M. Gupta).

0925-8388/$ – see front matter © 2011 Elsevier B.V. All rights reserved.
doi:10.1016/j.jallcom.2011.06.020

of microstructural and mechanical properties [6]. Accordingly, in the present study, 1.5 vol.% nano-sized alumina particulates were incorporated into newly developed AZ41 and AZ51 magnesium matrix and the influence of its addition on the microstructural, physical and mechanical properties of AZ41 and AZ51 was investigated.

2. Experimental procedures

2.1. Materials

In the present study, AZ31 magnesium alloy ingots (2.9% Al, 0.8% Zn, 0.6% Mn, 0.0023% Fe, 0.0011% Si, 0.0012% Cu, 0.0004% Ni and balance Mg) were used as a matrix material and cut into small pieces so that they can be placed into the graphite crucible easily. The aluminum lumps used were of 99.5% purity (supplied by Alfa Aesar, USA) and the reinforcement was in the form of 50 nm alumina powder of 99.4% purity (supplied by Baikowski, Japan).

2.2. Primary processing

Synthesis of monolithic AZ31, AZ41, and AZ51 alloys and their nanocomposites (incorporating 50 nm Al_2O_3) were carried out using disintegrated melt deposition (DMD) technique. Synthesis of AZ41 and AZ51 alloys involved heating the commercial AZ31 magnesium alloy pieces with the addition of 1 and 2 wt.% Al, respectively, while 1.5 vol.% alumina nano-particulates were added to synthesize their nanocomposites. Heating was performed at 750 °C under inert Ar gas atmosphere in a graphite crucible using a resistance heating furnace. The crucible was equipped with an arrangement for bottom pouring. Upon reaching the superheat temperature, the molten slurry was stirred for 5 min at 450 rpm using a twin blade (pitch 45°) mild steel impeller to facilitate the incorporation and uniform distribution of reinforcement particulates in the metallic matrix. The impeller was coated with Zirtex 25 (86% ZrO_2, 8.8% Y_2O_3, 3.6% SiO_2, 1.2% K_2O and Na_2O, and 0.3% trace inorganic) to avoid iron contamination of the molten metal. The melt was then released through a 10-mm diameter orifice at the base of the crucible. The composites melt were disintegrated by two jets of argon gas orientated normal to the melt stream. The argon gas flow rate was maintained at 25 L/min. The disintegrated composites melt slurry was subsequently deposited onto a metallic substrate. Preform of 40-mm diameter was obtained following the deposition stage. The synthesis of monolithic AZ31 magnesium alloy was carried out using steps similar to those employed for the reinforced materials except that no Al and reinforcement particulates were added.

2.3. Secondary processing

2.3.1. Pre-extrusion

The 40 mm diameter ingots were machined down using a lathe machine to a diameter of 36 mm and cut into billets with heights of approximately 45 mm. They were then lathed in the direction perpendicular to the length of the ingot to ensure both ends are flat and perpendicular to the surface. The billets were then sprayed with colloidal graphite for lubrication purposes.

2.3.2. Extrusion

The billets were first soaked at 400 °C for 60 min in a constant temperature furnace before extrusion. Extrusion was performed on a 150 tonne hydraulic press using an extrusion ratio of 20.25:1, producing rods of 8 mm diameter.

2.3.3. Post-extrusion

After extrusion, the extruded rods were machined to produce tensile specimens. Sections of approximately 10–15 mm in height were also cut by a low speed diamond blade and the surface graphite was then cleaned-off to use for various characterization studies.

2.4. Density and porosity measurement

Density measurements were performed in accordance with Archimedes' principle on four randomly selected polished samples taken from extruded rods [6,9]. Distilled water was used as the immersion fluid. The samples were weighed using an A&D HM-202 electronic balance with an accuracy of ±0.00001 g. Theoretical densities of materials were calculated assuming they are fully-dense and there is no Al_2O_3/AZ41 or AZ51 interfacial reaction to measure the volume percentage of porosity in the end materials. Rule-of-Mixture was used in all calculations. The porosity was calculated by using the theoretical and experimental densities.

2.5. Microstructural characterization

Microstructural characterization studies were conducted on metallographically polished extruded samples to investigate morphological characteristics of grains, reinforcement distribution and interfacial integrity between the matrix and reinforcement. The etching solution (5 ml acetic acid, 6 g picric acid, 10 ml water and 100 ml ethanol) was applied for approximately 20 s using a swabbing technique and then washed under running water to reveal the grain boundaries [20]. The sample was then analyzed using the Olympus BH2-UMA metallographic optical microscope equipped with Olympus DP-10 microscope digital camera. The grain boundaries were then traced out from the micrographs with the aid of the Adobe Photoshop program. Image analysis using the Scion system was carried out to determine the grain size of the materials.

The presence and distribution of the intermetallic phase was investigated using the JEOL JSM-5600LV Scanning Electron Microscope (SEM). Polished specimens were observed at 1000× magnification to reveal the intermetallic phase. Images were captured at an accelerating voltage of 15 kV and spot size of 20. The general distribution of the nano-sized alumina reinforcement was also investigated using the Hitachi S-4100 Field Emission Scanning Electron Microscope (FESEM). Metallographically polished specimens were used for this purpose.

2.6. X-ray diffraction studies

X-ray diffraction analysis of all samples was conducted using the automated Shimadzu LAB-X XRD-6000 X-ray diffractometer. Flat, ground and ultrasonically cleaned specimens of approximately 5 mm in height were exposed to CuK_α radiation (λ = 1.54056 Å) with a scanning speed of 2 °/min. The scanning range was 30–80° for all samples. A plot of intensity against 2θ (θ represents Bragg angle) was obtained, illustrating peaks at different Bragg angles. The Bragg angles corresponding to different peaks were noted, and the values of interplanar spacing (d-spacing) obtained from the computerized output were compared with the standard values from the International Centre for Diffraction Data's Powder Diffraction File (PDF).

2.7. Coefficient of thermal expansion

The coefficients of thermal expansion (CTE) of all the compositions were determined by measuring the displacement of the samples as a function of temperature in the temperature range of 50–400 °C using an automated SETARAM 92-16/18 thermo-mechanical analyzer.

2.8. Mechanical testing

The mechanical properties of all samples were investigated by conducting tensile and microhardness tests. All experiments were carried out at room temperature.

2.8.1. Microhardness

The microhardness tests were conducted on flat and metallographically polished specimens. The tests were conducted using a Shimadzu HMV automatic digital microhardness tester with a Vickers indenter (square-based pyramidal-shaped diamond indenter with face angle of 136°). An indenting load of 25 gf and a dwell time of 15 s were used. Testing was performed in accordance with ASTM test standard E384-08. Indentations were made and measurements were recorded in Vickers Hardness (HV).

2.8.2. Tensile testing

The tensile properties of each sample were determined in accordance with ASTM test standard E8M-08. Round tension test specimens of 5 mm in diameter were machined from the 8 mm extruded rod. An average of five tensile specimens could be obtained from a single rod, and a minimum of four tensile tests were conducted for each sample. Tests were performed on the 810 Material Test System (MTS) with an extensometer of 25 mm gauge length and a crosshead speed of 0.254 mm/min was used. The raw stress–strain data recorded was extracted to be analyzed. Broken test specimens were labeled individually, carefully handled and packed into individual plastic bags to prevent damage to the fractured surface. A Microsoft Excel program was written to analyze the raw data extracted. Then, 0.2% offset yield strength (0.2% YS), ultimate tensile strength (UTS) and failure strain (FS) was computed via a series of Microsoft Excel functions. The work of fracture (WoF) was also computed in the program by the use of the trapezium rule.

2.9. Fracture behavior

The fracture surfaces of the broken tensile samples were analyzed to investigate the failure mechanisms that occurred during the tensile tests. Fractography studies were performed on the JEOL JSM-5600LV Scanning Electron Microscope. Images were captured at an accelerating voltage of 15 kV and a working distance of about 25 mm. Macromechanism of these fracture surfaces were also investigated.

3. Results and discussion

3.1. Primary processing

Synthesis of new AZ series magnesium alloys and their nanocomposites were successfully accomplished by the disintegrated melt deposition. Observations of the deposited ingots before secondary processing revealed that there was no detectable reaction between the graphite crucible and melts, minimal oxidation on the

Table 1
Results of density and porosity measurements of AZ series alloys and their nanocomposites.

Compositions	Al (wt.%)	Al_2O_3 (vol.%)	Density (g/cm^3)		Porosity (%)
			Theoretical	Experimental	
AZ31	–	–	1.776	1.775	0.05
AZ41	1.0	–	1.786	1.785	0.05
AZ51	2.0	–	1.792	1.791	0.08
AZ41–Al_2O_3	1.0.	1.5	1.818	1.816	0.10
AZ51–Al_2O_3	2.0	1.5	1.827	1.825	0.09

melts and an absence of blowholes and macropores. These observations are consistent with previous findings made on Mg based composites synthesized using DMD method [6,9,11,19] and verified the suitability of using DMD as the primary processing method for this study.

3.2. Secondary processing

The extrusion parameters used in the present study were selected based on previous studies [6,9,11]. The successful extrusion of AZ41 and AZ51 magnesium alloys and their nanocomposites without a drastic increase in pressure applied indicates that the extrusion parameters were adequate and ensured uniform plastic flow of the material.

3.3. Density and porosity measurement

The experimental density obtained by the Archimedes' principle exhibited that the density of newly developed magnesium based materials increased negligibly with the addition of elemental Al and alumina nano-size particulates into AZ31 matrix (see Table 1). This can be attributed to the higher density of Al (2.70 g/cm^3) and Al_2O_3 (3.96 g/cm^3) when compared to AZ31 matrix (1.78 g/cm^3) [1,6]. Obtained results also revealed that the experimental values were relatively close to the theoretical values. This indicated that the experimental methodology used in this study is capable of producing near dense materials.

Porosity of the materials was calculated using the theoretical and the experimental densities obtained from each sample. The highest porosity obtained among the samples was 0.10% (see Table 1), hence indicating that near dense materials were obtained and that the alloying constituent and the reinforcement were successfully incorporated into the matrix. Therefore, as demonstrated in prior studies, the fabrication route of DMD followed by hot extrusion is capable of producing nanocomposites with minimal porosity [6,19,21].

3.4. Microstructural characterization

Results of microstructural characterization of all extruded samples are shown in Tables 2 and 3 and in Figs. 1 and 2 and discussed in terms of: (a) grain morphology, (b) the presence, distribution and morphology of the second phase particles, (c) presence and distribution of reinforcing particles and (d) the matrix/reinforcements interfacial bonding. Microstructural characterization results revealed the presence of near-equiaxed grains for all samples indicating its independency on the incorporation of nano-sized alumina particles and/or addition of aluminum into AZ31 magnesium alloy (see Table 2 and Fig. 1). β-$Mg_{17}Al_{12}$ phase predominantly located at grain boundaries was observed in all samples (see Fig. 1). Average grain size decreased with the addition of elemental Al into AZ31 matrix. This can be attributed to the pinning of grain boundaries by the increasing amount of second phases resulting in limited grain growth. On the contrary, the addition of 1.5 vol.% nano-sized Al_2O_3 particulates along with Al in AZ31 magnesium had minimal effect in reducing grain size (when compared to AZ31) suggesting the incapability of nano-Al_2O_3 particulates to serve as either nucleation site or obstacles to grain growth during solid state cooling. However, the variation of grain size is statistically insignificant considering standard deviation for all samples.

SEM micrographs of the etched samples revealed the presence and good distribution of the equilibrium intermetallic phase $Mg_{17}Al_{12}$. SEM analysis revealed that the nano-sized alumina particulates in the AZ/Al_2O_3 systems were found to exist both in small clusters and also individually distributed in the matrix (see Fig. 2). Even in the clusters, the alumina particulates were found to be individually spaced and distributed, and the clusters themselves were fairly evenly distributed in the matrix (see Fig. 2(f)). This can be attributed to the use of a layered arrangement of the raw materials during the solidification process and effective stirring parameters. The successful disintegration of the melt and the inert atmosphere caused by the argon gas jets were also the contributing factors. In the AZ41 and AZ51 samples, the intermetallic particles appeared to have sharp edges. At these boundaries, the local stress concentration will be higher than that of the AZ31 system, which has blunt edges (see Fig. 2). Addition of the nano-sized alumina particulates in AZ41 and AZ51 helped to blunt the edge of intermetallic phase by breaking down them, thereby lowering the local stress concentration (see Fig. 2). Results of microstructural characterization also revealed good interfacial integrity between Al_2O_3 and matrix (see Fig. 2(f)), absence of debonded regions and interfacial reaction products. The results are consistent with the previous observations made on Mg/Al_2O_3 nanocomposite formulations [6,19].

Table 2
Results of grain morphology of AZ series alloys and their nanocomposites.

Compositions	Grain size (μm)	aspect ratio	Roundness[a]
AZ31	4.1 ± 1.8	1.5 ± 0.4	1.5 ± 0.4
AZ41	2.9 ± 1.3	1.6 ± 0.4	1.6 ± 0.6
AZ51	2.8 ± 1.3	1.7 ± 0.5	1.7 ± 0.7
AZ41–Al_2O_3	3.8 ± 1.6	1.7 ± 0.5	1.5 ± 0.3
AZ51–Al_2O_3	3.6 ± 1.5	1.7 ± 0.5	1.6 ± 0.4

[a] Roundness is the shape of the grain expressed by the formula (perimeter)^2/4π (area).

Table 3
Results of X-ray diffraction (XRD) and coefficient of thermal expansion (CTE) analysis.

Compositions	XRD (no. of matching peaks)		CTE (μm/mK)
	Mg	$Mg_{17}Al_{12}$	
AZ31	11	1	28.8
AZ41	11	2	27.1
AZ51	10	2	27.0
AZ41–Al_2O_3	10	3	26.5
AZ51–Al_2O_3	10	3	26.2

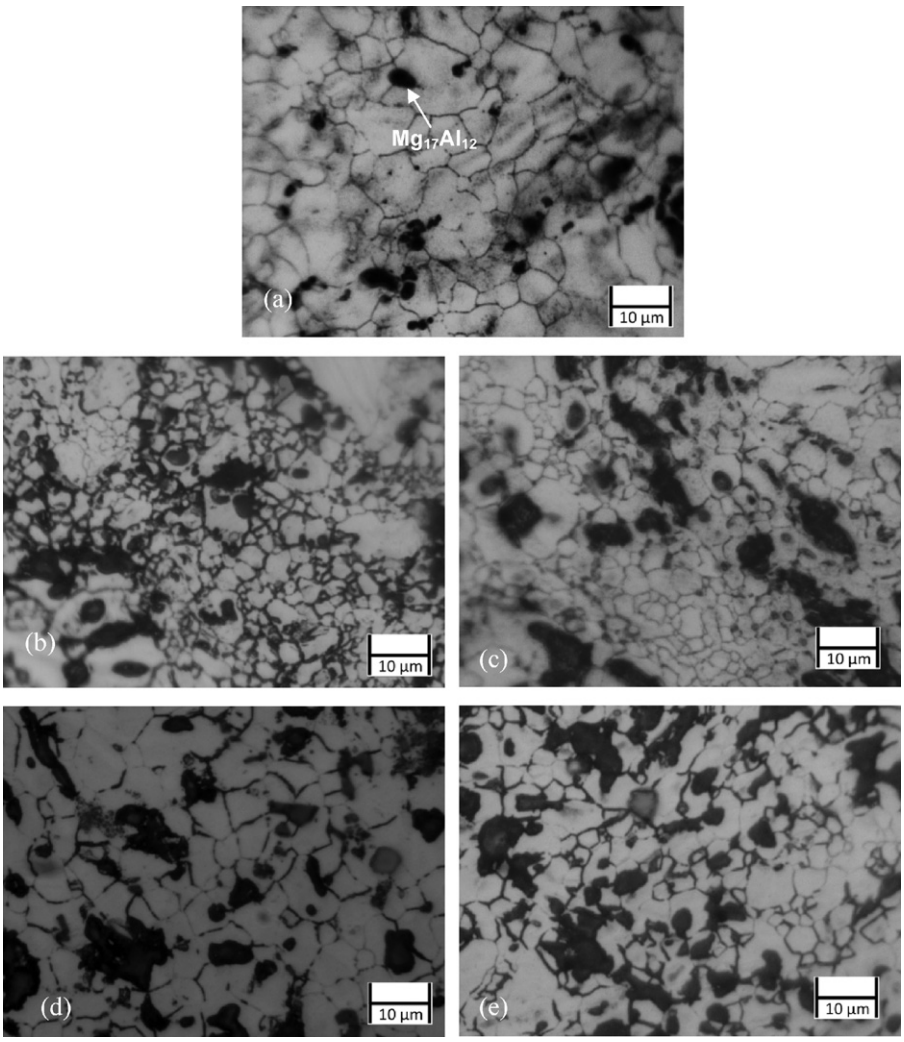

Fig. 1. Representative optical micrographs showing the grain morphology (1000×) of: (a) AZ31, (b) AZ41, (c) AZ51, (d) AZ41–Al_2O_3 and (e) AZ51–Al_2O_3 samples, respectively.

3.5. X-ray diffraction

X-ray diffraction (XRD) studies were carried out on all extruded and polished samples (see Table 3). The obtained lattice spacings (d-spacing) and two-theta (2θ) value were compared with the standard values for magnesium and the Mg–Al intermetallic phases. X-ray diffraction results confirmed the presence of the intermetallic phase β-$Mg_{17}Al_{12}$ in all of the compositions (see Table 3 and Fig. 3). For the AZ/Al_2O_3 nanocomposites, the increased number of intermetallic peaks can be observed indicating higher amount of second phase formed when compared to the Mg–Al systems. However, no peaks corresponding to nano-sized alumina were present. This can be attributed to the limitation of the filtered X-ray to detect phases with amount less than 2 vol.% [9,22].

3.6. Coefficient of thermal expansion

Table 3 shows the results of coefficient of thermal expansion measurements obtained from AZ31, AZ41, AZ51alloys and nanocomposites. The results of CTE measurement showed that the addition of Al and the subsequent addition of nano-sized alumina particulate reinforcement decreased the average CTE values of the composites (see Table 3). This can be attributed to the lower CTE value of Al ($23.6 \times 10^{-6}\,K^{-1}$) [1] and Al_2O_3 ($7.0 \times 10^{-6}\,K^{-1}$) [4] when compared to monolithic AZ31 alloy and the ability of the reinforcements to effectively constrain the expansion of the matrix. The results of the AZ/Al_2O_3 systems suggested an appropriate integration of AZ alloys with nano-sized alumina particulates leading to low CTE values as demonstrated in prior studies [6]. The results are consistent with similar findings made by investigations on other magnesium based formulations containing different types of reinforcements and in different length scales [19,23].

3.7. Mechanical characteristics

3.7.1. Microhardness

The experimental results of microhardness measurement are shown in Table 4. AZ31 magnesium exhibited the lowest average hardness value and the average microhardness increased by about 29% with the addition of 2 wt.% Al in AZ31. This can be attributed to the lower average grain size of AZ51 when compared to AZ31 which is associated with larger grain boundary area leading to higher hardness [24]. A prominent increase (~67%) in microhardness was observed in AZ51–Al_2O_3 nanocomposite sample when compared to unreinforced AZ31 (see Table 4). This is consistent with the earlier observations made on Mg–Al_2O_3 nanocomposite formulations [6,19,23]. The increase in hardness of nanocomposite in the present study can be attributed to: (i) the reasonably uniform distribution of harder Al_2O_3 nano-particulates in the matrix, and (ii) higher constraint to the localized matrix deformation during indentation due to the presence of the nano-particulates [6,18,19,23,25]. Moreover, the microhardness value of AZ51–Al_2O_3 nanocompo-

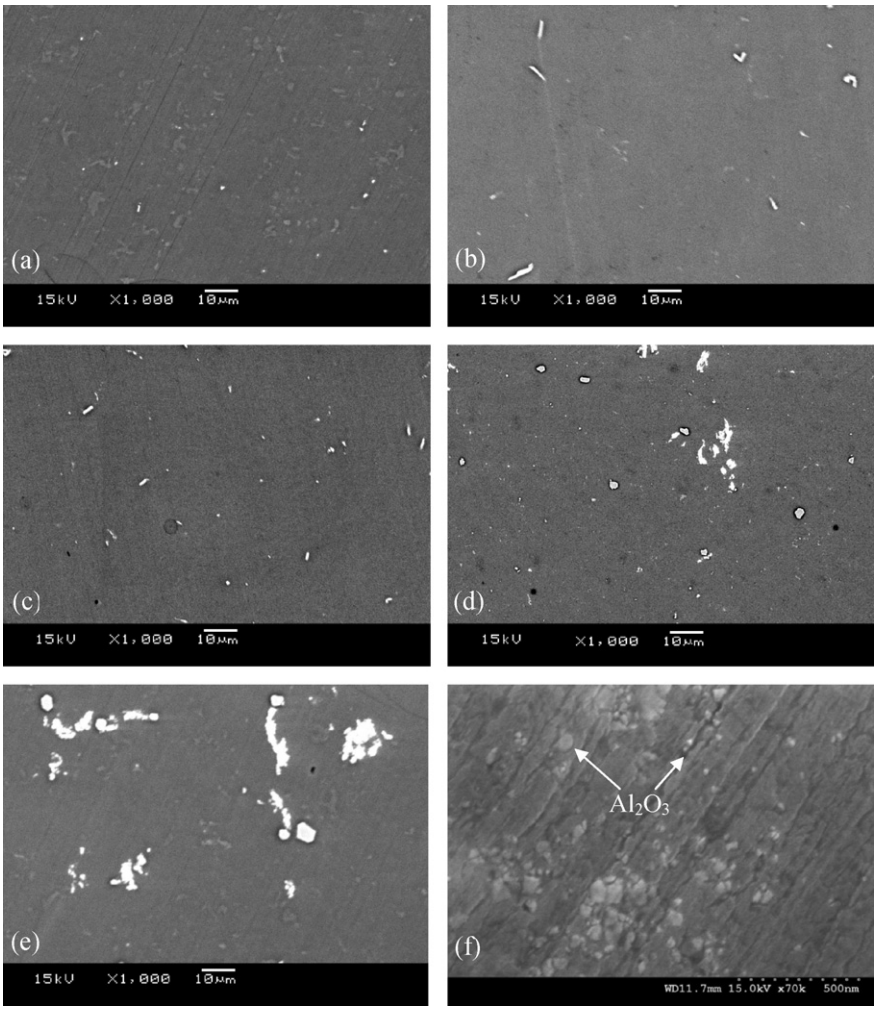

Fig. 2. Representative SEM micrographs showing the shape and distribution of second phase and reinforcements in the case of: (a) AZ31, (b) AZ41, (c) AZ51, (d) AZ41–Al_2O_3 and (e) AZ51–Al_2O_3 samples, respectively. (f) Represents the FESEM micrograph of the nano-sized alumina distribution in the case of AZ41–Al_2O_3 sample.

site was much higher than pure Mg (~182%) and pure Al (~120%) developed under the same processing parameters (see Table 4) [26].

3.7.2. Tensile testing

Room temperature tensile test results revealed that the addition of Al increased the strength of monolithic AZ31 magnesium alloy (~23% increment of 0.2% YS and ~11% increment of UTS in case of 2 wt.% Al addition) (see Table 4 and Fig. 4). This can be attributed to the lower average grain size of AZ41 and AZ51 samples when compared to AZ31 samples (see Table 2 and Fig. 1). Presence of additional Al modified the microstructural features, hence increasing strength. Increase in strength can also be attributed to: (a) the increased presence of uniformly distributed $Mg_{17}Al_{12}$ phase and (b) the effective transfer of applied tensile load to the well-bonded $Mg_{17}Al_{12}$ phase (see Fig. 2) [9]. This follows a trend as the strength level of AZ61, AZ80 and AZ91 is higher than that

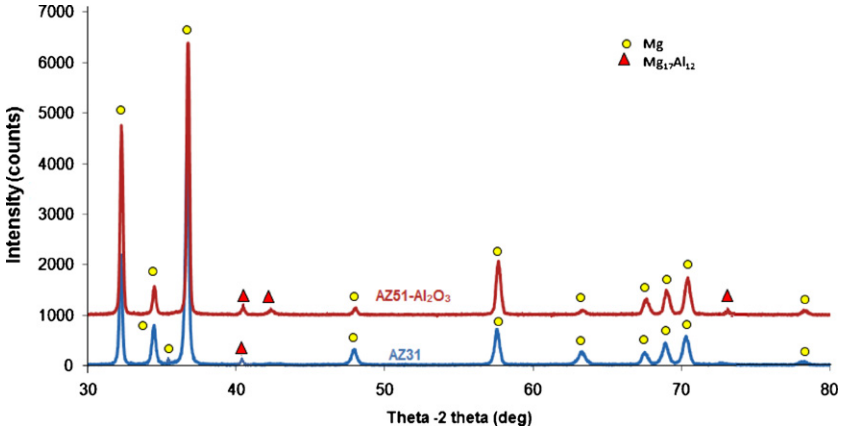

Fig. 3. X-ray diffractogram of AZ31 and AZ51–Al_2O_3 samples showing β-$Mg_{17}Al_{12}$ second phase in the α-Mg matrix phase.

Table 4
Results of room temperature microhardness and tensile properties of AZ series alloys and their nanocomposites.

Compositions	Microhardness (HV)	0.2% YS (MPa)	UTS (MPa)	FS (%)	WoF (MJ/m^3)
AZ31[a]	66 ± 2	180 ± 3	273 ± 6	10.6 ± 1.3	27.9 ± 3.9
AZ41[a]	77 ± 3	218 ± 5	287 ± 6	8.2 ± 0.3	23.0 ± 1.4
AZ51[a]	85 ± 3	222 ± 4	302 ± 4	8.7 ± 0.4	27.3 ± 1.2
AZ41–Al_2O_3[a]	98 ± 3	200 ± 2	302 ± 3	12.3 ± 1.2	36.0 ± 3.5
AZ51–Al_2O_3[a]	110 ± 3	211 ± 4	311 ± 3	13.4 ± 1.2	40.7 ± 3.1
AZ31–Al_2O_3 [6][a]	86 ± 3	144 ± 9	214 ± 16	29.5 ± 1.9	60 ± 3
AZ61 [1][a]	62	230	310	16	–
AZ80 [27][a]	–	248	338	12	–
AZ91 [9][a]	–	272 ± 3	353 ± 0	3.7 ± 0.5	–
ZK21 [28][a]	–	195	260	4	–
ZK31 [28][a]	–	210	295	7	–
M2 [27][a]	–	160	215	4	–
WE43 [27][a]	–	160	260	6	–
WE54 [27][a]	–	180	280	6	–
AZ91 [28][b]	–	145	275	6	–
ZK61 [28][b]	–	185	310	–	–
Mg [26][a]	39 ± 2	124 ± 11	201 ± 13	6.1 ± 1.1	11.6 ± 2.6
Al [26][a]	50 ± 3	137 ± 9	183 ± 8	19.4 ± 0.3	32.6 ± 1.4

[a] Extruded samples.
[b] Sand cast samples.

of AZ31 alloy [1,9,27]. Moreover, the tensile strength of AZ41 and AZ51 alloys was much better than: (a) selected wrought/cast Zr-free (or Al-containing) Mg alloys having similar or higher Al content, (b) selected wrought/cast Zr-containing (or Al-free) Mg alloys, (c) commercially available manganese containing wrought Mg alloy, (d) magnesium–yttrium–rare earth alloys (WE-alloys) and (e) pure Mg and Al, as listed in Table 4 [1,27,28]. Failure strain decreased with Al addition into AZ31 magnesium. This can be attributed to the formation and presence of sharp edge intermetallic particles which might act as a stress concentration sites (see Fig. 2). WoF also dropped for AZ41 magnesium when compared to AZ31 magnesium. This can be attributed to the lower area under the stress–strain curve as the ductility of AZ41 is lower than AZ31. However, WoF of AZ51 samples remain unchanged when compared to AZ31 and increased when compared to AZ41 samples.

The results of tensile properties characterization on nanocomposite samples showed that the presence of nano-sized alumina particulates in AZ41 and AZ51 slightly decreased the 0.2% YS and marginally increased the UTS. Decrease in strength (0.2% YS) of nanocomposites may be attributed to: (a) the relatively larger average grain size of AZ–Al_2O_3 nanocomposites when compared to their respective AZ alloys (see Table 2), (b) the modification of intermetallic particulate morphology from sharp edged to the blunt edged (see Fig. 2), and (c) the presence of some clusters of Al_2O_3 which might cause the clustered region to yield at a lower macroscopic stress during uniaxial tensile loading (see Fig. 2) [29]. However, the strength of AZ-1.5Al2O3 nanocomposites was much higher than that of monolithic AZ31 magnesium and some other commercially available wrought and cast magnesium alloys (see Table 4). A significant increase (50–54%) in failure strain was observed in the AZ–Al_2O_3 nanocomposites when compared to their respective AZ alloys. This increment can be attributed to: (i) the presence and reasonably good distribution of the reinforcements, and (ii) the reduction in local stress concentration present in the matrix due to the blunt shape of the intermetallic states. Dispersed phases in brittle matrix, where dislocation mobility is restricted and crack propagation is relatively easy, act as ductility enhancer, an anomaly to their effect in ductile matrix [30]. Dispersed reinforcement particulates in brittle metal matrix serve to: (a) provides sites where cleavage cracks may open ahead of an advancing crack front, (b) dissipate the stress concentration which would otherwise exist at the crack front, and (c) alter the local effective state of stress from plane strain to one of plane stress in the neighbourhood of the crack tip. In addition, it has been understood through different studies that nano-sized Al_2O_3 reinforcements have the ability to activate non-basal slip system at room temperature in magnesium based matrix under axial tensile stress and helps to increase ductility [6,31]. Work of fracture expresses the ability of material

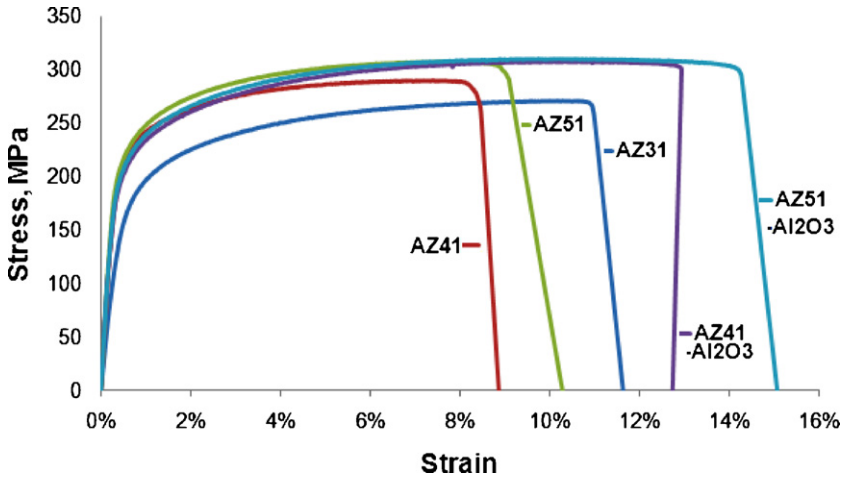

Fig. 4. Engineering stress–strain diagrams of AZ31, AZ41, AZ51 alloys and their Al_2O_3 nanocomposites.

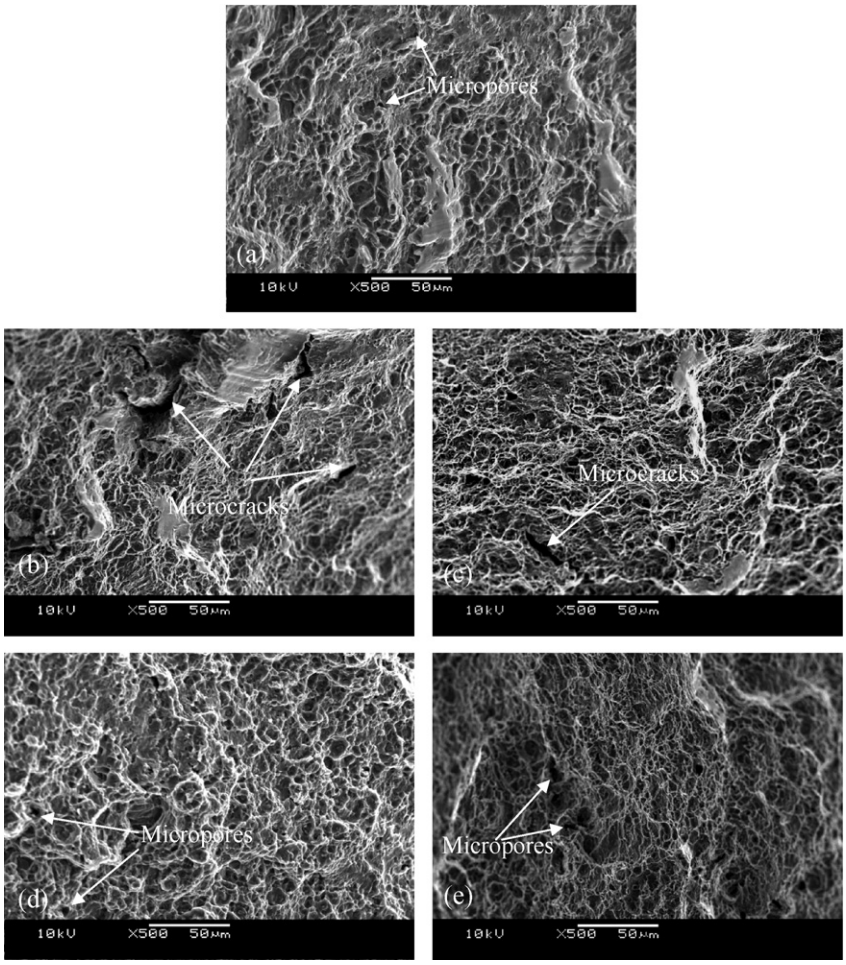

Fig. 5. Representative SEM fractographs showing the micropores and dimple like features for: (a) AZ31, (d) AZ41–Al_2O_3 and (e) AZ51–Al_2O_3 samples, while (b) AZ41 and (c) AZ51 samples showing microcracks along with micropores and dimples.

to absorb energy up to fracture under tensile load and corresponds to the area under engineering stress–strain curve [19]. The work of fracture of the nanocomposites was found to be much higher when compared to their respective AZ magnesium alloys and improved by around 50–57% (see Table 4). This can mainly be attributed to the improved failure strain of the nanocomposite samples synthesized in the present study. The results thus clearly reveal the enhanced damage tolerant capability of AZ41 and AZ51 magnesium alloys when reinforced with Al_2O_3 particulates in nano-length scale.

The tensile results further revealed that the addition of nano-sized alumina and/or elemental Al into AZ31 magnesium alloy exhibited better specific 0.2% YS and UTS when compared to the AZ31 alloy (see Table 5). AZ51–1.5Al_2O_3 nanocomposite exhibited much higher specific strength (~45% higher 0.2% YS and ~44% higher UTS) when compared to AZ31–1.5Al_2O_3 nanocomposite processed under the same condition. Furthermore, these newly developed AZ/Al_2O_3 nanocomposites exhibit superior specific strength when compared to pure Mg, Al and steel and thus can be used as a valuable structural material for weight critical applications [1–5].

Table 5
Results of specific strengths of AZ series alloys and their nanocomposites.

Compositions	$\sigma_{0.2\%YS}/\rho$	σ_{UTS}/ρ
AZ31	101	154
AZ41	122	161
AZ51	124	169
AZ41–Al_2O_3	110	166
AZ51–Al_2O_3	116	170
AZ31–Al_2O_3[a]	80	118
Mg[a] [26]	71	116
Al[a] [26]	51	68

[a] Considering 1.738 g/cm^3 and 2.70 g/cm^3 are the density of Mg and Al, respectively [1].

3.8. Fracture behavior

Macroscopic observations performed on the broken tensile samples revealed shear type fracture characteristics. Microscopic observations showed that dimple like features were predominately presented in all compositions, indicating significant plastic deformation (see Fig. 5). However, relatively higher presence of microcracks along with micropores were observed in the AZ41 and AZ51 systems which are responsible for the decrease in failure strain of these composites when compared to AZ31 samples. Relatively lesser presence of micropores along with absence of microcracks in the tensile fractured images of nanocomposite samples are responsible for high plastic deformation of AZ–Al_2O_3 nanocomposites. Dimple like features are more prominent in the nanocomposite fractographs, represent the evidence of higher ductility of these compositions.

4. Conclusions

The following conclusions can be made from the present study:

1. Monolithic AZ31, AZ41, AZ51 magnesium alloys and their Al_2O_3 containing nanocomposites can be successfully synthesized by using the disintegrated melt deposition technique followed by hot extrusion with minimal porosity.
2. The microstructure of the newly developed AZ alloys and their nanocomposites consist of the α-Mg phase and the intermetallic β-$Mg_{17}Al_{12}$ phase. The presence of nano-sized alumina assists in the breaking down of the intermetallic phase and decreases its sharpness and helps to reduce local stress concentration.
3. The coefficient of thermal expansion of AZ31 magnesium decreases with the addition of elemental aluminum. The addition of nano-sized alumina particulates further helps to decrease the CTE values.
4. Microhardness values increase with the elemental Al addition as an alloying element to AZ31 magnesium, and further increases with the addition of nano-sized alumina particulates.
5. Room temperature tensile test reveals that the addition of Al into AZ31 significantly increases both the engineering and specific 0.2% yield strength and ultimate tensile strength, but decreases the failure strain while work of fracture remains almost unchanged. The addition of 1.5 vol.% nano-sized alumina particulates along with 1–2 wt.% Al in the AZ31 system helps to increase the 0.2% yield strength and the ultimate tensile strength noticeably when compared with AZ31 magnesium. The failure strain and work of fracture of the nanocomposite increases significantly with the addition of the nano-sized reinforcement.

Acknowledgment

The authors gratefully acknowledge the support received for this research work ref: NPRP 08-424-2-171 from the Qatar National Research Fund (QNRF), Qatar.

References

[1] J.R. Davis, Properties and Selection: Nonferrous Alloys and Special-Purpose Materials, Formerly Tenth Edition, ASM Handbook, vol. 2, ASM, Metal Park, Ohio, 1993, pp. 457, 480–515, 1099–1100, 1118–1128, 1199, 1132–1135.
[2] B.L. Mordike, K.U. Kainer, Magnesium Alloys and Their Applications, Werkstoff-Informationsgesellschaft, Frankfurt, Germany, 1998.
[3] B.L. Mordike, T. Ebert, Mater. Sci. Eng. A 302 (2001) 137–145.
[4] D.J. Lloyd, Int. Mater. Rev. 39 (1994) 1–23.
[5] F. Moll, K.U. Kainer, in: K.U. Kainer (Ed.), Magnesium Alloys and Technology, Wiley-VCH, Weinheim, 2002, pp. 197–217.
[6] Q.B. Nguyen, M. Gupta, J. Alloys Compd. 459 (2008) 244–250.
[7] A. Martin, J. Llorca, Mater. Sci. Eng. A 201 (1995) 77–87.
[8] W. Westengen, Magnesium: Alloying, in: K.H.J. Buschow, R.W. Cahn, M.C. Flemings, B. Ilschner, E.J. Kramer, S. Mahajan, P. Veyssière (Eds.), Encyclopedia of Materials: Science and Technology, Elsevier, 2008, pp. 4739–4743.
[9] S.F. Hassan, K.F. Ho, M. Gupta, Mater. Lett. 58 (2004) 2143–2146.
[10] K. Hirai, H. Somekawa, Y. Takigawa, K. Higashi, Mater. Sci. Eng. A 403 (2005) 276–280.
[11] Q.B. Nguyen, M. Gupta, J. Compos. Mater. 43 (2009) 5–17.
[12] Presentations from Elektron 21 product launch CD provided by Magnesium Elektron, UK, http://www.magnesium-elektron.com/site-map.asp (accessed on 13 March' 2011).
[13] X. Gong, H. Li, S.B. Kang, J.H. Cho, S. Li, Mater. Des. 31 (2010) 1581–1587.
[14] H.M. Chen, H.S. Yu, S.B. Kang, G.H. Min, Adv. Mater. Res. 79–82 (2009) 2139–2142.
[15] S. Wang, M. Wang, R. Ma, Y. Wang, Y. Wang, Rear Met. 29 (2010) 396–400.
[16] K. Matsuzaki, K. Hatsukano, Y. Torisaka, K. Hanada, T. Shimizu, M. Kato, Mater. Sci. Forum 539–543 (2007) 1747–1752.
[17] B.H. Kim, J.J. Jeon, K.C. Park, B.G. Park, Y.H. Park, I.M. Park, Int. J. Cast Met. Res. 21 (2008) 186–192.
[18] C.S. Goh, J. Wei, L.C. Lee, M. Gupta, Nanotechnology 17 (2006) 7–12.
[19] S.F. Hassan, M. Gupta, J. Mater. Sci. 41 (2006) 2229–2236.
[20] A. Jager, P. Lukac, V. Gartnerova, J. Haloda, M. Dopita, Mater. Sci. Eng. A 432 (2006) 20–25.
[21] S.F. Hassan, M. Gupta, Mater. Sci. Technol. 20 (2004) 1383–1388.
[22] B.D. Cullity, Elements of X-Ray Diffraction, 3rd ed., Prentice Hall, London, 2001.
[23] S.F. Hassan, M. Gupta, J. Alloys Compd. 419 (2006) 84–90.
[24] G.E. Dieter, Mechanical Metallurgy, 2nd ed., McGraw-Hill, Inc., USA, 1976, pp. 191–193.
[25] M. Gupta, M.O. Lai, D. Saravanaranganathan, J. Mater. Sci. 35 (2000) 2155–2165.
[26] M. Paramsothy, N. Srikanth, M. Gupta, J. Alloys Compd. 461 (2008) 200–208.
[27] H.E. Friedrich, B.L. Mordike, Magnesium Technology: Metallurgy, Design Data, Applications, Springer-Verlag Berlin Heidelberg, Germany, 2006, pp. 210–212, 302–310.
[28] M.M. Avedesian, H. Baker, ASM Specialty Handbook: Magnesium and Magnesium Alloys, ASM International®, Ohio, 1999, pp. 12–25, 165–172, 226–248, 258–263.
[29] W.W.L. Eugene, M. Gupta, Adv. Eng. Mater. 7 (2005) 250–256.
[30] G.S. Ansell, in: R.W. Cahn (Ed.), Physical Metallurgy, North-Holland Publishing Company, Netherlands, 1970.
[31] S.F. Hassan, M. Gupta, J. Alloys Compd. 429 (2007) 176–183.